Received: 4 November 2024 | *Revised:* 4 January 2025 | *Accepted:* 7 January 2025
DOI: 10.37917/ijeee.22.1.38 *Vol. 22 | Issue 1 | June 2026*

Iraqi Journal for Electrical and Electronic Engineering
Original Article

Open Access
IJEEE University of Basrah College of Engineering

Local Frequency Restoration-Based Communication-Free Approach in Islanded Microgrids

Ali Shamkhi*, Basil H. Jasim
Electrical Engineering Department, Universtiy of Basrah, Basrah, Iraq

Correspondance
*Ali Shamkhi
Electrical Engineering Department, Universtiy of Basrah, Basrah, Iraq
Email: alishamki21@gmail.com

Abstract
Reducing the dependency of the control system on communication in the microgrid increases the reliability and flexibility of an islanded microgrid. This paper presents a local secondary control approach to provide a fast response to power change and accurate frequency restoration. It is based on a control scheme that uses a secondary controller involving a time-controllable parameter for a Low pass filter. The high value of the time-varying parameter is placed to satisfy excellent performance regarding fast active power sharing, and the time-controllable parameter decreases after achieving power-sharing based on a time protocol to ensure accurate steady-state frequency restoration. This paper also describes the criteria for control parameter selection and stability analysis based on a precise modeling approach. The MATLAB environment is used to simulate and test the proposed control scheme, and the results have been obtained that show the validity and high performance of the proposed controller in terms of dynamic response to active power change and steady-state restoration under different operation conditions.

Keywords
Event-Driven Strategy, Hierarchical Control, Secondary Control, Time-Dependent Protocol.

I. Introduction

The distribution of parallel inverter's energy to the system load is a primary goal of the microgrid control system, and this goal is achieved by using the droop control method in the islanded operation of the microgrid [1–4]. The frequency deviation occurs at a steady state due to the droop control method. This steady-state deviation can be corrected using a secondary control strategy, where the secondary control layer modifies the droop equation to ensure accurate restoration while keeping the power-sharing. Many secondary control strategies are used to provide accurate steady-state frequency restoration, such as centralized and distributed communication approaches (see [5, 6]). These strategies require data exchanges between Distributed generators to provide accurate power sharing with accurate frequency restoration.

The centralized communication approach is the conventional approach for correcting the frequency deviation. The microgrid central control measures and compares the bus variables with their reference values. The standard PI controller calculates the secondary term and then distributes it to all DGs connected to the microgrid [7]. The problem with the one-to-all communication approach is the dependency on the single point to calculate control action, leading to a single failure point problem [8, 9].

The distributed communication approach overcomes this limitation by using an all-to-all or neighbor-to-neighbor communication system [10], where each DG determines the secondary term locally based on local and neighbor information [11]. Generally, the distributed secondary control eliminates the dependency on the central controller. The averaging technique is one of the distributed secondary control approaches, which involves high-traffic data exchange between DGs, leading to an all-to-all communication system [12]. In this approach, the average frequency is calculated at each local controller by collecting the frequencies of other DGs, and the frequency error is estimated and manipulated via a stan-

This is an open-access article under the terms of the Creative Commons Attribution License,
which permits use, distribution, and reproduction in any medium, provided the original work is properly cited.
©2026 The Authors.
Published by Iraqi Journal for Electrical and Electronic Engineering | College of Engineering, University of Basrah.

dard PI controller. Another approach to distributed secondary control is the consensus algorithm, which is based on MAS and uses a neighbor-to-neighbor communication system [13]. The consensus algorithm reduces the number of communication links between DGs, increasing the microgrid system's flexibility and reliability. However, centralized and distributed communication approaches require a communication system to compute the secondary control action.

The limitations of using a communication system refer to time delays, high-traffic scheduling, transmission period, sampling and quantization scheme, and the difficulty of physical implementation, especially when the number of DGs increases [14, 15].

To overcome the communication problems and increase the flexibility of the microgrid control system, the communication-free control system is used where each DG controller calculates its correction term. Only local information is used to satisfy active power sharing and frequency restoration [16–22]. The communication system is necessary for a multi-layer control scheme, especially in the tertiary layer or during the black start processes. However, reducing dependency on communications in each layer of the control system increases system reliability. The traditional no-communication approach uses a standard PI controller at each DG unit, the estimated local frequency compares with the nominal frequency value, leading to local frequency restoration. Unfortunately, this approach suffers from a hunting problem due to the parallel operation of the PI controller in each DG unit. The instability issue is introduced by referring to hunting phenomena that occur as a result of the integration action of the controller. There are many potential solutions to satisfy stable local restoration.

In [23, 24], the multi-layer control system without communication can operate with either grid-connected or grid-forming converters proposed; the local frequency restoration based on modifying the droop equation via controlling virtual impedance is described in [25].

This paper presents a communication-free secondary control system based on event-driven with time-controllable parameters. The instability problem is compensated using an adaptable low-pass filter with a proper mechanism to avoid a hunting phenomenon. The proposed control scheme involves two cases: the large value of the time-varying parameter to ensure a fast dynamic response and the small value to provide an accurate steady-state restoration.

This approach provides the following advantages: (1) accurate and fast response for active power changes, (2) accurate steady-state restoration, and (3) improvement of the flexibility and reliability of the microgrid control system. (4) Eliminating the dependency on the central controller. Only the communication approaches can simultaneously ensure accurate active power-sharing and accurate frequency restoration. The proposed scheme validation was tested using the MATLAB environment. This paper is classified as follows: Section II discusses Paper Contributions, and Section III describes the review of the DG control structure for the islanded microgrid. Section IV discusses the proposed control scheme (secondary control based on a time-controllable parameter via a Low Pass filter) with stability analysis and parameter design, and the simulation results are reported in Section V. Finally, Section VI shows general conclusions.

II. Paper Contribution

The proposed control scheme's major contributions include the absence of communication links between DGs and eliminating dependency on MGCC. It balances transient response to active power changes and steady-state frequency restoration. Table I summarize the major contribution of our work.

III. Distributed Generator Control Review

In grid-connected mode, the control scheme is implemented to control on a grid-following converter, where the utility grid feeds the active power. Then, the converter behaves as a power-controlled current source. The grid-forming converters must be used when the microgrid disconnects from the main grid [26]. The hierarchical control scheme controls the microgrid grid-forming converters in islanded mode. The overall microgrid structure is shown in Fig. 1. The droop control method is considered the basic method for providing power sharing and stabilizing frequency and voltage amplitude. The steady-state frequency deviation occurs due to the droop control method. The steady-state deviation is corrected using a secondary control layer [27, 28]. The tertiary layer manages and optimizes the power flows to satisfy economic considerations [29–33].

A. Voltage and Current Representation Frame

Natural reference frame representation of voltage and current leads to difficulties in the control system. Three control channels are required to control and synchronize three-phase quantities. Transformation of the measured voltage and current of the three-phase inverter into the stationary reference frame facilitates the control process. Control improvement refers to reducing the number of control channels, which are two separate channels. These quantities are controlled using a proportional-resonant controller (PR), the proportional-resonant controller is discussed in the paper [34]. The synchronization is necessary to convert the three-phase signal from the natural reference frame (abc-reference frame) to two

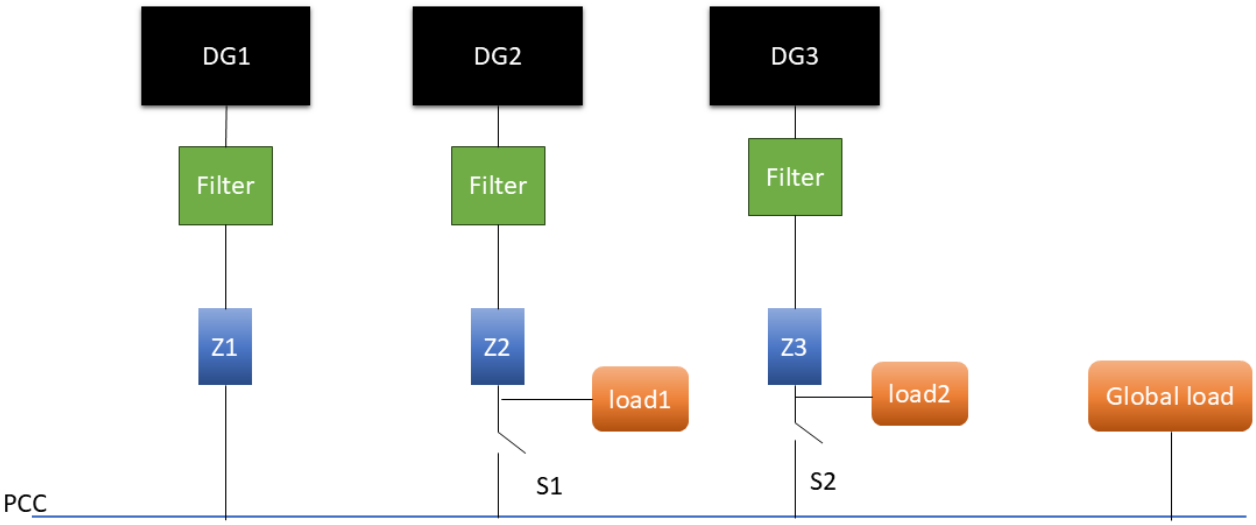

Fig. 1. Overall Microgrid Scheme

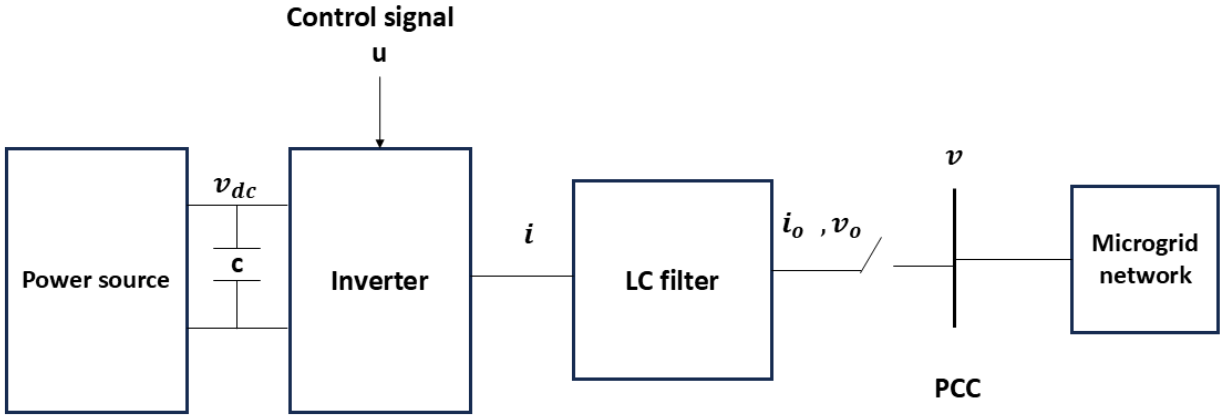

Fig. 2. Power source interfacing with microgrid

TABLE I.
COMPARISON BETWEEN PROPOSED CONTROL SCHEME WITH PREVIOUS WORKS

Control startegy	Active power sharing	Frequency restoration	Depedency on MGCC	Communication netwrok
Paper [9]	accurate	accurate	strong	High
Paper [12]	accurate	accurate	not required	High
Paper [13]	accurate	accurate	not required	Moderated
Paper [16]	accurate	not accutare	not required	not required
Our Work	accurate	accurate	not required	not required

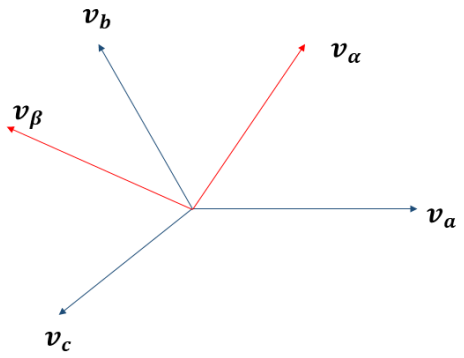

Fig. 3. Natural reference frame and a stationary reference frame vector representation

orthogonal components. A phase-locked loop (PLL) synchronizes the local voltage with the microgrid bus voltage. The mathematical transformation from a natural reference frame to a stationary reference frame is called the Clarck transformation. In a natural reference frame, each phase is delayed by 120° from another phase, while in a stationary reference frame, the phase α and β are separated by 90°.

$$\begin{bmatrix} v_\alpha \\ v_\beta \\ v_\gamma \end{bmatrix} = \begin{bmatrix} \frac{2}{3} & -\frac{1}{3} & -\frac{1}{3} \\ 0 & \frac{1}{\sqrt{3}} & -\frac{1}{\sqrt{3}} \\ \frac{1}{3} & \frac{1}{3} & \frac{1}{3} \end{bmatrix} \begin{bmatrix} v_a \\ v_b \\ v_c \end{bmatrix}$$

B. DG Control Scheme

In an islanded microgrid, the primary control layer is the upper layer and the fastest layer in the multi-layer control strategy. This control layer performs active power-sharing and frequency stabilization.Fig. 4. shows the overall primary control scheme. A droop control method is a conventional approach that is used to regulate the angular frequency (w) by controlling the output active power (P), and the output reactive power (Q) is reduced to regulate the voltage amplitude (V). The operation of the droop method is summarized in (1) and (2), where w_r represent the reference angular frequency, v_r represents the reference voltage amplitude, and m and n are the droop gains since (i=1,2,3….N), where N represents the number of DGs connected to the microgrid. Fig. 5. shows the linear relationship between active power and frequency.

$$w_i = w_r - m_i P_i \tag{1}$$

$$v_i = v_r - n_i Q_i \tag{2}$$

The low pass filter is necessary to separate between dynamics of control layers, where LPF filters the instantaneous active and reactive power with a cutoff frequency w_d.

$$\frac{w_d}{s + w_d} \tag{3}$$

$$v_i = v_r - n_i Q_i \tag{4}$$

The frequency is a global variable of the microgrid. The power-sharing between converters is done equally when the droop coefficient m has the same value for all DGs connected to the microgrid. The droop method can be improved to ensure accurate steady-state active power-sharing with accurate frequency restoration. This modification is done by using a supervisory control layer, and accurate reactive power-sharing is challenging to achieve due to dependency on the voltage profile, where the voltage is a local variable that leads to creating a trade-off between reactive power-sharing and voltage profile, leading to established small voltage deviation. However, This paper focuses on active power sharing and steady-state frequency restoration, compensating voltage deviation, and ensuring reactive power sharing is out of the scope of this paper. The reference sinusoidal signal is created using the droop equations' angular frequency and voltage amplitude.

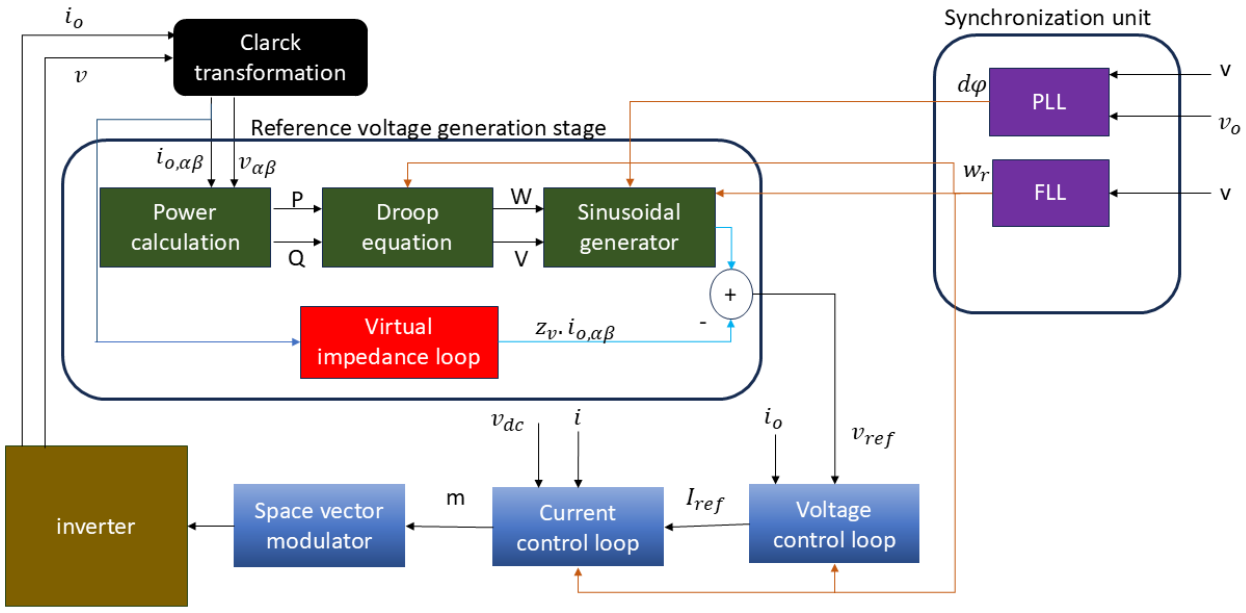

Fig. 4. The overall primary control scheme

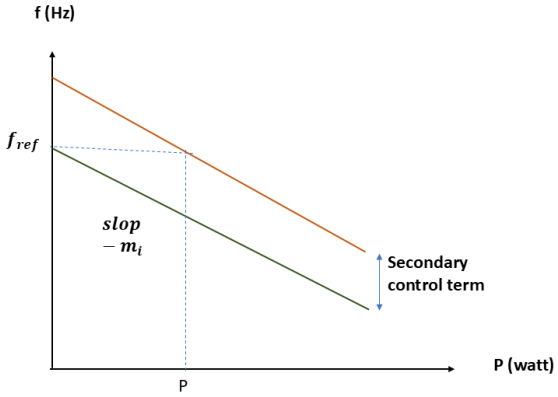

Fig. 5. Droop characteristics and secondary control action

The reference sinusoidal signal generated at each converter is described by (5)

$$v_{ref} = v_i sin(w_i * t) - z_v i_o \tag{5}$$

The voltage amplitude was produced by a droop equation at each converter v_i represent the amplitude of the reference sinusoidal signal, the angular frequency w_i modify to fastest the transient response of active power during changes, this modification is done by adding feed-forward gain to the nominal frequency, the derivative term used to improve closed-loop pole locations and increasing damping features.

$$w_i = w_r - m_i P_i - m_{ip} \frac{dp}{dt} \tag{6}$$

The virtual impedance term is necessary to improve the droop method functionalities by reducing the effects of circulating current and reducing distortion. The virtual impedance involves two terms R_v and L_v , the modification of reference sinusoidal signal as shown in (7).

$$v_{ref} = v_i sin(w_i t) - (R_v i_o + L_v \frac{di_o}{dt}) \tag{7}$$

The main function of the voltage control loop is to track the converter's output voltage with reference AC sinusoidal voltage signal generated by the sinusoidal Reference generation stage. The voltage represented by the stationary reference frame leads to established two control channels. Each control channel involves two compensators to provide full tracking with reference ac sinusoidal signal v_{ref} , the first compensator is used to track the fundamental component of AC sinusoidal reference voltage. In contrast, the harmonic compensator attenuates the harmonic components of a sinusoidal reference voltage. Both compensators behave as a bandpass filter with a narrow band of frequencies of interest [35]. The FLL is used to adapt the cutoff frequency for these filters. This adaptation improves the performance of these compensators, especially when a significant deviation occurs in the microgrid. The output current of the converter is entered as a feed-forward

signal to the voltage control loop to accelerate the transient response during fast changes.

The current control loop receives the AC reference current from the voltage tracking control loop. Then, the current tracking loop tracks the output current of the converter with the reference current generated by a voltage control loop. This control loop uses the same producer used with the voltage control loop and has some additional features. The design considerations of these compensators include (1) ensuring the high sensitivity of the Bandpass filter and (2) separating the bandwidth of control loops, where the bandwidth voltage control loop must be slightly lower than the current control loop, to avoid overlap and ensure fast voltage tracking.

The secondary control action is done by modifying the droop equations and adding an extra term$\delta$to the basic droop equations. The modified equation is as follows:

$$w_i = w_r - m_i P_i + \delta \tag{8}$$

Several secondary control approaches can be used to calculate the secondary term. These approaches are classified according to using communication systems. The centralized and distributed control approaches are based on communications to calculate secondary action [36, 37]. However, some approaches, such as event-driven strategy, do not require communication to determine secondary action.

C. Synchronization Unit of the Microgrid Control Scheme

The local controller of each DG is involved PLL unit to synchronize the output voltage of the converter (v_o) with microgrid voltage (v). A PLL does not operate when the converter disconnects from the microgrid; the operation of a PLL starts when the converter is ready to connect to the microgrid. The phase increment $d\phi$ produced by a PLL feeds to the basic equation of reference voltage, the modified reference signal after applying this term to the basic equation of reference voltage shown in (9)

$$v_{ref} = v_i sin(w_i t - m_{pi} P_i + d\Phi) - (R_v i_o + L_v \frac{di_o}{dt}) \tag{9}$$

Accurate implementation of PLL is necessary to avoid high current overshoot when the switch is closed. The cross-product approach is the simple synchronization method used for implementing a PLL, where the cross-product signal must be reduced to zero.Equation (10) shows the mathematical representation of cross product approach in a stationary reference frame

$$v_c^2 = v_{o\alpha} v_\beta - v_{o\beta} v_\alpha \tag{10}$$

A sinusoidal AC signal may produce harmonics and noise. A low-pass filter is necessary to prevent any noise coming from the cross-product operation. The standard PI controller is used to reduce the cross-product signal to zero. Fig. 6. shows the block diagram of PLL internal components.

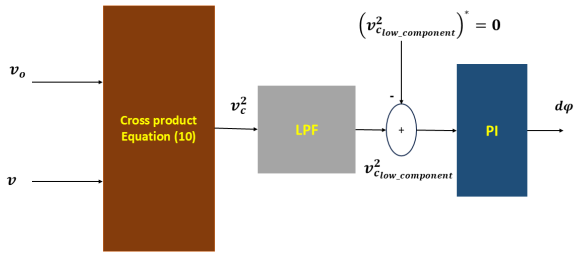

Fig. 6. Block diagram of the internal PLL structure.

IV. Proposed Control Strategy

The first-order low-pass filter is used for determining the secondary control term according to the following equation

$$\delta = \frac{w_s}{s + k w_s}(w_r - w_i) \tag{11}$$

Where k is the control parameter of the low pass filter, and w_s represents the cutoff frequency of a low pass filter.

From (8) and (11), the steady-state frequency error can be expressed as follows:

$$e_{ss} = w_r - w_i = \frac{kmP}{1+k} \tag{12}$$

Both (11) and (12) show that both deviation equation and steady-state error depend on the control parameter k. The proposed control strategy allows for a design trade-off between dynamic response and steady-state accuracy. The value of k undergoes the time protocol for controlling the bandwidth of the low pass filter, the large value of parameter k leads to a fast transient response with inaccurate steady-state frequency restoration during a defined period, and the small value of parameter k leads to accurate frequency restoration with low speed of transient response. The event-triggering mechanism of a secondary control system involves three basic stages: event detection stage, time-protocol activation, and deviation calculation stage. Fig. 7. shows the block diagram for calculating the secondary term using an event-driven mechanism.

A. Switching State of Secondary Term

The time-varying parameter takes a large value called k_{max} to satisfy the fast dynamic response during the power-sharing period, this refers to the high value of parameter k, which means

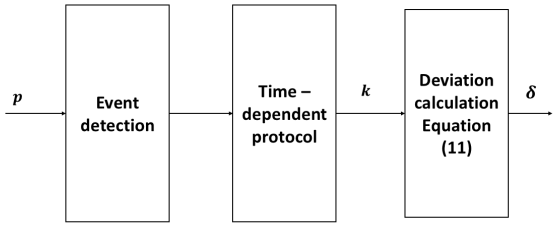

Fig. 7. Block diagram for event-driven mechanism.

a high bandwidth of a low pass filter. After that, the value of parameter k must slightly decrease to a minimum value called k_{min} for achieve accurate steady-state frequency restoration. The low bandwidth of a low-pass filter is associated with a minimum value of parameter k. The values of k_{max} and k_{min} should be selected carefully to avoid problems related to stability in transient response and the hunting phenomena during the steady-state period; the design considerations are discussed in another section.

$$\delta = \begin{cases} \frac{w_s}{s+k(t)w_s}(w_r - w_i) & for\ k \geq k_{min} \\ \frac{w_s}{s+k_{min}w_s}(w_r - w_i) & for\ k = k_{min} \end{cases} \quad (13)$$

B. Event-Triggering Strategy

An event detection strategy is necessary for the proposed control scheme. Using an event detection strategy improves the performance of the proposed control system, especially with multi-event scenarios. The send-to-delta is the most common approach to detect the changes based on threshold value [38]. The active power of each voltage source inverter must be checked locally, and the sampling should be done over each converter's active power. When the percentage of active power changes exceeds the threshold value, then the event is triggered. The threshold value increment should be designed carefully to ensure accurate change detection and avoid unreal events. The event detection conditions can also depend on the change in frequency to catch the event. In this paper, the event detection strategy uses the change in active power as an inductor to the event, which refers to this approach as more appreciable, leading to easier to identify.

C. Time-Dependent Protocol

Once the event occurs, the parameter k varies according to a specific pattern. A time protocol with some constraints drives this pattern. Fig. 8. shows the time protocol of single-event and multi-event scenarios.

At the beginning of the pattern, at (t=t_e) the maximum value of k, namely k_{max} must assigned to ensure a fast transient response with a high steady-state error during a time period called T_p , at (t=t_c) the parameter k changes from it is maximum value k_{max} to minimum value k_{min} during period called T_r , during the linear transition from k_{max} to k_{min}a low steady-state error is ensured with a low speed of transient response, at (t=t_r) the parameter k is adjusted to the minimum value until the next event occurs. (14) summarizes the behavior of the k parameter in the time-dependent protocol.

$$k(t) = \begin{cases} k_{\max} & \text{if } t_e \leq t < t_e + T_p \\ k_{\max} + \frac{k_{\min} - k_{\max}}{t_r}(t - t_e - T_p) & \text{if } t_e + T_p \leq t < t_e + T_p + T_r \\ k_{\min} & \text{if } t \geq t_e + T_p + T_r \end{cases} \quad (14)$$

D. Design Guidelines

The design involves the parameters of the proposed secondary approach that are represented by (1) the maximum value of parameter k (k_{max}), minimum value of parameter k (k_{min}),(3) power-sharing interval in a time-dependent protocol T_p ,(4) steady-state restoration interval in time-dependent protocol $T_r)$, (5) the threshold value of the event detection mechanism Δp.

Firstly, a very high value of parameter k leads to overshooting in power-sharing, while a low value leads to a slow transient response. According to (12), the parameter k_{max} should determine the allowed maximum frequency error $e_{ss,max}$

$$k_{max} = \frac{m_i P_{max} - e_{ss,max}}{e_{ss,max}} \quad (15)$$

where P_{max} represents the maximum power delivered by DGs in a microgrid, selecting of parameter k_{min} is a critical issue. The fault in frequency restoration may occur referring to a large value of k_{min} , when k_{min} close to zero, the integral action of the filter is dominated, leading to hunting problems due to the parallel operation of the voltage source inverter. The frequency error in a steady state must have a small value $e_{ss,d}$, the parameter k_{min} should determine the desired steady-state frequency error. From (12), the formulation of k_{min} shown as below

$$k_{min} = \frac{m_i P_{max} - e_{ss,d}}{e_{ss,d}} \quad (16)$$

The changes in active power should exceed the threshold value Δp to activate the time-dependent protocol, the threshold value should be designed suitably to ensure accurate event detection. The changes are not detected when the large threshold value is assigned, and the small value considers the measurement noise and oscillation that may lead to a lying event being

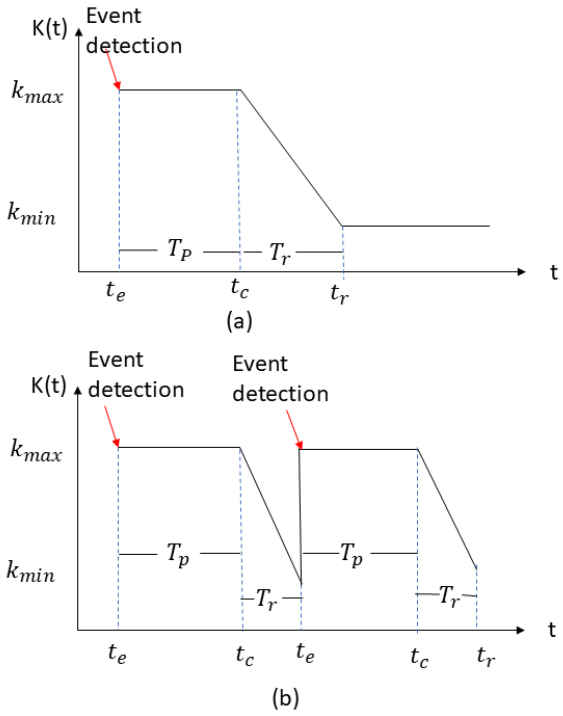

Fig. 8. Time-dependent protocol: (a) single event scenarios, (b) multievent scenarios

triggered. Once the event is fired, the maximum allowed error is assigned

$$e_{ss,\max} = \frac{m_i}{1+k_{\max}} p_i(t_e) \tag{17}$$

The desired steady-state error is assigned at the restoration period

$$e_{ss,d} = \frac{m_i}{1+k_{\max}} p_i(t) \tag{18}$$

From (17) and (18), the maximum error change is

$$d_{e_{ss}} = \Delta p \frac{m_i}{1+k_{\max}} = e_{ss,\max} - e_{ss,d} \tag{19}$$

The threshold value should be takes upper bound

$$\Delta p \leq (de_{ss}) \frac{m_i}{1+k_{max}} \tag{20}$$

The overall interval of the time-dependent protocol is defined by T_c, whereT_c is a combination T_p and T_r , this value should be more significant than the primary layer response. The fast transient response of active power is done by increasing the k parameter to it is the maximum value for a period defined as T_p , T_p is the time interval for achieving accurate power sharing, the value of T_p is specified according to the desired settling time of the transient response of active power, the slope interval $T_r$should be equal to or larger than the power-sharing period T_p to balance operation between power sharing and a steady state frequency restoration, the total time response of primary layers is 1 sec, the better choice is to select T_c=10 sec , to provide an excellent trade-off between power sharing and frequency restoration, the same value assigned to T_p and T_r.Our assumption of time period values as T_p =T_r= 3 sec.

E. Stability Analysis

Fig. 9 shows the equivalent circuit of the DG with microgrid bus voltage. The output voltage of the converter is defined as

$$v(t) = V\sin(wt + \varphi)$$

and the bus voltage is represented as

$$v_{bus}(t) = v_{bus}\sin(wt)$$

The DG unit connects to the main voltage bus via coupling impedance Z. The coupling impedance can be calculated by considering the output impedance of DG and the virtual impedance. If inductive behavior is dominant in coupling impedance with assuming the angle φ close to zero ($\sin(\varphi) \approx$

φ), the output active power of the converter can be calculated as below:

$$p = \frac{3}{2}\frac{V v_{bus}}{Z}\varphi \tag{21}$$

The variable parameter k significantly influences microgrid stability. Since instability can occur due to a combination of stable systems, the ordinary stability method that depends on the location of closed-loop poles is inefficient [39].

The Lyapunov function can represent the desired range of parameter k. The plant and control laws are described as follows:

$$\dot{x} = Ax \tag{22}$$

The closed-loop state matrix is represented by matrix A, and the state vector x is defined as $[P, \delta, q]$. The following procedures are used to formulate the closed-loop state matrix.

From (3) and (21), the output active power is described as below:

$$P(s) = \frac{3}{2}\frac{w_d}{s+w_d}\frac{V v_{bus}}{Z}\varphi \tag{23}$$

The inverse Laplace transform is used to transform active power

$$\frac{dp}{dt} = -w_d P + \frac{3}{2}\frac{V v_{bus}}{Z}\varphi \tag{24}$$

The inverse Laplace transform is used to transform the proposed secondary control equation that is described by (11):

$$\frac{d\delta}{dt} = m w_s sgn(k) P - w_s(1+sgn(k))\delta \tag{25}$$

It is known the angular frequency represents the derivative of the phase angle

$$w = \frac{d\varphi}{dt} = \frac{d(w_r t + \varphi)}{dt} = w_r + \frac{d\varphi}{dt}$$

$$w - w_r = \frac{d\varphi}{dt} \tag{26}$$

From (26) and (8)

$$\frac{d\varphi}{dt} = -mP + \delta \tag{27}$$

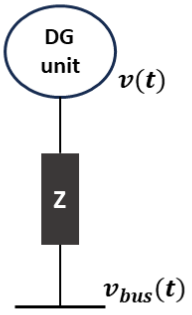

Fig. 9. Equivalent circuit of an interface of DG system to microgrid.

The closed-loop state transfer matrix can be written according to (24), (25), and (27).

$$A = \begin{bmatrix} -w_d & 0 & \frac{3}{2}\frac{V v_{bus}}{Z} w_d \\ m w_s & -w_s(1+k)sgn(k) & 0 \\ -m & 1 & 0 \end{bmatrix} \tag{28}$$

The Lyapunov function for parameter-varying linear systems is represented as follows:

$$V(x) = x^T M x \tag{29}$$

For the specific range of k parameter values should be determined, with M satisfying

$$A^T M + MA < 0 \tag{30}$$

For the values of k that are limited from 0.01 to 0.4, these values make the matrix M a positive definite matrix

$$M = \begin{bmatrix} 0.00005 & -0.02 & -0.23 \\ -0.02 & 36.4 & 23.1 \\ -0.23 & 23.1 & 11873.5 \end{bmatrix}$$

V. Simulation Results

The MATLAB Simulink environment is used to implement the microgrid scheme shown in Fig. 1. The switches state sequence as follows: DG1 directly connects to the microgrid with global load, and after (5 sec) DG3 and load2 are entered by closing switch 2, then load sharing begins. At 10 sec, switch 1 close, connecting DG2 and load1. Finally, load2 leaves the microgrid at 30 sec.

TABLE II. ELECTRIC PARAMETER OF MICROGRID SCHEME

Parameter	Symbol	Quantity
Reference angular frequency	W_r	$2\pi \times 50$ rad/s
Reference voltage amplitude	v_{ref}	$110 \times \sqrt{2}$ V
Filter inductor	L_f	5 mH
Filter capacitor	C_f	10 μF
Line impedance 1	Z_1	$0.065 + j2\pi \times 10^{-3}\Omega$
Line impedance 2	Z_2	$1.2 \times Z_1\Omega$
Line impedance 3	Z_3	$1.2 \times Z_1\Omega$
Sampling time	T_s	$1e^{-6}$ sec
Global Load	$Z_{globale\_L}$	$20 + j2\pi \times 0.05\Omega$
Load 1	Z_{load1}	5 kW
Load 2	Z_{load2}	10 kW

A. Primary Control Layer Test

The parameter design involves the primary control parameters that are represented by droop gain m and feed-forward gain mp , and the virtual impedance loop. Firstly, the droop gain for active power m is selected to satisfy accurate active power-sharing according to the angular frequency of each DG. Equation (31) shows the calculation of a droop parameter for active power, where P_{max} represent the maximum active power delivered by each DG and dw_i the steady state frequency error.

$$m_i = \frac{dw_i}{P_{max}} \tag{31}$$

$$n_i = \frac{dw_i}{2Q_{max}} \tag{32}$$

accurate active power sharing is done by adjusting $m_1P_1 = m_2P_2 = m_3P_3$ at steady state, the better droop gains value of the frequency droop equation to achieve accurate power sharing is chosen as the same values for each local controller $m_1 = m_2 = m_3 = 130 * 10^{-6} rad/(watt.sec)$, the same producer with the voltage regulation droop equation, the design of the n parameter does not ensure accurate reactive power-sharing due to the voltage variety for each DG, accurate reactive power sharing is not an issue in this paper. The instantaneous active and reactive power is filtered by using a first-order low-pass filter with a cutoff frequency w_d , the value of w_d is selected to ensure the separation of the primary from other control layers in a multilayer control scheme. In this paper, the cutoff frequency of power of a low pass filter is adjusted as $3\pi rad/second$. The feed-forward gain m_p should be selected as a small value to avoid the overshooting in transient response during the power-sharing interval; the very large value of feed-forward gain leads to a delay in transient response and destroys the sinusoidal waveform. In this paper value of a parameter m_p is selected as $10 * 10^{-6}$ rad/watt, Fig. 10. shows the sinusoidal reference voltage with different values of feed-forward gain. The virtual impedance must be modified to satisfy pure inductive behavior, the inductive effect must be dominant to achieve excellent compensation, and the design equations of virtual impedance focus on increasing the impedance angle θ to larger than 65°.

$$\theta = \tan^{-1}\left(w_r \frac{L}{R}\right) > 65^\circ \tag{33}$$

Where L consists of two terms the virtual inductance combined with microgrid inductance $(L_v + L_g)$, and R is the combination of virtual resistance and microgrid resistance $(R_v + R_g)$. The microgrid system operates with a primary control layer only. According to (1) and (2), accurate active power sharing refers to dependency on frequency. The results in Fig. 13. The primary control layer is presented. The time scope of microgrid operation with the primary layer is described as follows: At the start of microgrid operation in Islanded mode, the DG1 connects to the microgrid with the global load, which generates the maximum active power of about 7800 watts. The DG3 connects to the microgrid with load2 after 5 sec is passed, and the active power sharing is done, where the value of the microgrid active power decreases to 4350 watts. DG2 enters the microgrid at 10 sec. The active power is stabilized at 3400 watts until reached at 30 sec with 3100 watts, where the frequency restoration takes ranges between 49.7 Hz and 50.1 Hz, the first second approximately the frequency is adjusted to 49.80 Hz, and after passing 5 sec the frequency slightly changes 49.9 Hz, the value of 49.95 be dominating for a period from 10 sec to 30 sec, finally at 30 sec the frequency be closer to 50 Hz. The deviation value is approximately about 0.05 for each power change in active power. The compensation of this steady-state deviation is necessary by using a supervisory control layer.

TABLE III. PRIMARY CONTROL PARAMETERS

Parameter	Symbol	Quantity
Active power droop gain	m	$130 \times 10^{-6} \frac{\text{rad}}{\text{sec·watt}}$
Reactive power droop gain	n	$1 \times 10^{-4} \frac{\text{volt}}{\text{VAR}}$
Feed-forward gain	m_p	$10 \times 10^{-6} \frac{\text{rad}}{\text{watt}}$
Virtual impedance	z_v	$0 + j2\pi \times 0.001\Omega$
Proportional gain of voltage compensator	k_{pv}	0.1
Integral gain of voltage compensator	k_{iv}	0.1
Damping rate of voltage compensator	ξ_v	0.01
Proportional gain of the current compensator	k_{pi}	12
Integral gain of the current compensator	k_{ii}	200
Damping rate of the current compensator	ξ_i	0.01
Primary cutoff frequency	w_d	$0.3 \times 2\pi \times 50 \frac{\text{rad}}{\text{sec}}$

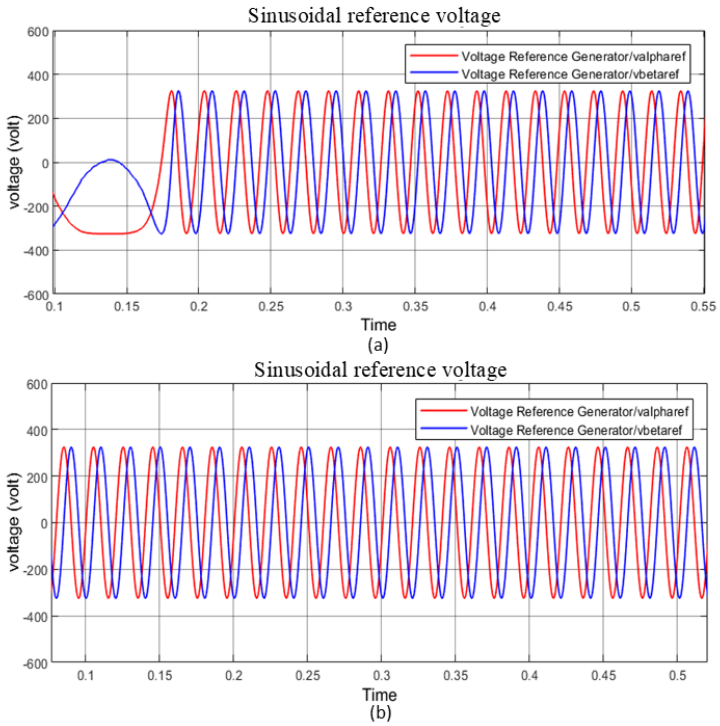

Fig. 10. The reference voltage signal (a) with $(m_p = 10 * 10^{-3} rad/watt)$,(b)with $(m_p = 10 * 10^{-6} rad/watt)$.

B. Proposed Secondary Control Scheme Test

Testing with a secondary control layer based on the parameter varying via a low-pass filter was performed. The same frequency droop gain parameter was selected for all DGs connected to the microgrid.

1) Testing without Time-Dependent Protocol

Assuming the maximum allowed frequency error is equal to the desired error at a steady state $e_{ss,max} = e_{ss,d} = 0.15$, then the maximum value of parameter k will be assigned $k = k_{max}$, the primary control layer test shows that the maximum active power of DGs is 7840 watts, the value of k=0.4 according to (15), by applying the maximum value of k along the transient response time of the secondary control layer without considering the time-dependent protocol, the proposed control system will provide accurate power sharing without any frequency restoration. Fig. 12. shows that once the event is triggered, the fast transient response of active power is done accurately; on the other hand, the frequency deviation is not compensated during the operation of the secondary control layer. At 5 sec, DG3 enters the microgrid with load2 to share its power with DG1, and both DGs cooperate to contribute 4800 watts to the load. At 10 sec, DG3 is connected to a microgrid, and then the droop method of the local controller operates to share its power with other DGs to contribute 3400 watts to the Islanded microgrid. On the other hand, steady-state frequency restoration is not done. For a period (0 to 5 sec), the frequency deviation is approximately 0.15. After that, the deviation decreases to 0.13 as a result of connecting DG3 to the Microgrid. At 10 sec, the frequency deviation is stable at 0.11, as shown in part (b) from Fig. 12.

2) Testing without Time-Dependent Protocol $(k = 0.01)$

Assuming the small value assigned to the k parameter value $k = k_{min} = 0.01$ irrespective of time-dependent protocol, as shown in part (c) from Fig. 13, then the desired steady-state error becomes $e_{ss,d} \simeq 0.01$. By applying the minimum value of k along the timescale of the secondary control layer without considering the time-dependent protocol, the proposed control system will restore the frequency for each change that occurs in a microgrid. On the other hand, the slow transient response leads to the failure of accurate power sharing. Fig. 13. shows that once the event is triggered, the steady state frequency is compensated accurately; on the other hand, power sharing is not satisfied during the operation of the secondary control layer due to a slow dynamic response. At 5 sec, DG3 entered the microgrid with load2 and synchronized with DG1, the settling time of transient response elapsed 2 sec, and a similar problem occurred at 10 sec when DG2 was connected, as shown in part (a) from Fig . 13. The steady-state error is

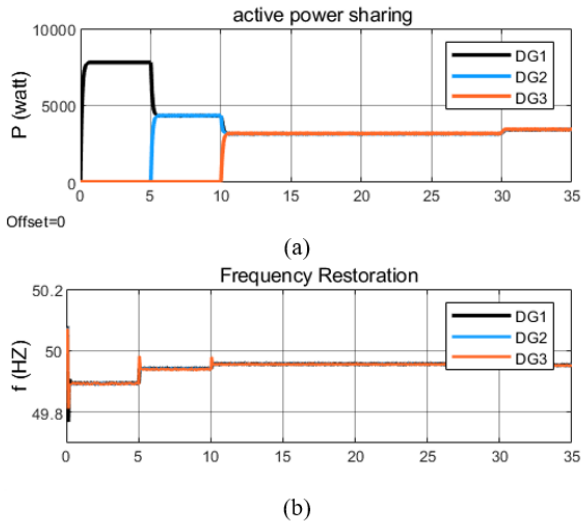

Fig. 11. (a) Active power-sharing of the primary control layer, and (b) frequency restoration of the primary layer.

closer to zero along microgrid operation, as shown in part (b) from Fig. 13.

3) Testing with Time-Dependent Protocol $(0.01 \leq k \leq 0.4)$

The time-dependent protocol is activated based on the event detection mechanism, assuming the allowed maximum frequency error during a power-sharing period is 0.15, while the desired frequency error at a steady state period is 0.01. According to (15) and (16), the parameter k takes two values $(k_{max} = 0.4)$and $(k_{min} = 0.01)$, the maximum value will be assigned during the transient response period (T_p), and the minimum value of parameter k is assigned during the steady-state restoration period (T_r). According to (20), the threshold value should be larger than 0.0003. Fig. 14 shows that once the event is triggered, the fast transient response provides accurate active power sharing irrespective of a steady-state error. After passing 3 sec, the speed of the transient response gradually decreases while frequency restoration starts until it reaches its nominal value through 2 sec only. At 5 sec, DG3 entered the microgrid with load2 and synchronized with DG1. Here, the settling time of transient response is very short as a result of the High Bandwidth of the low-pass filter due to time-protocol execution. At the same time, the steady-state error decreased from its maximum value to zero during 3 sec, as shown in part (b) from Fig. 14. The producer of time protocol, which is shown in part (c) from Fig. 14 repeated for each change in active power.

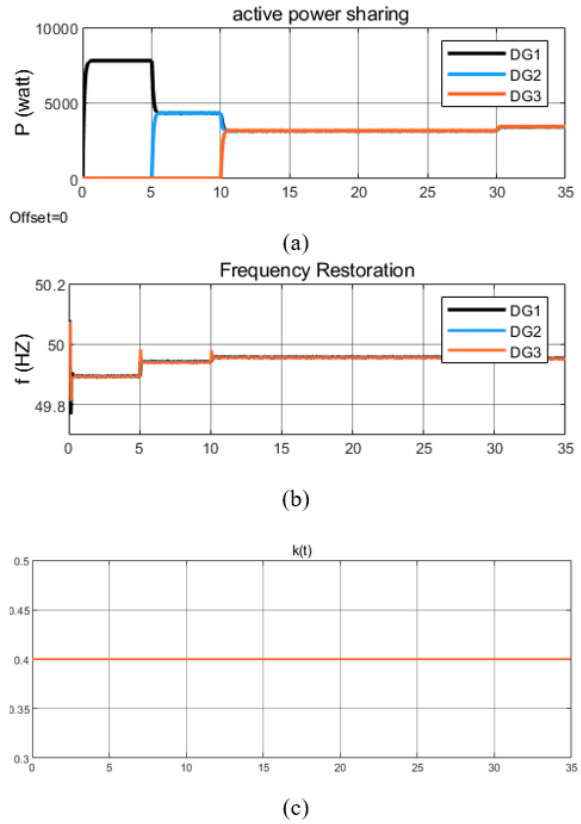

Fig. 12. (a) Active power-sharing of the proposed control scheme for k=0.4,(b) frequency restoration of the proposed control scheme for k=0.4, (c) time-dependent protocol of parameter k.

VI. Conclusion

This paper proposes a local no-communication secondary control approach for islanded microgrids. The proposed control scheme is based on a time-driven protocol to change the filter bandwidth of the low-pass filter when the changes occur. The proposed time protocol maximizes the value of the time-varying parameters during the transient interval and decreases to a minimum value during the steady state period. With this suggested system, the reliability and flexibility of the microgrid are increased. The results show the ability of the proposed control scheme to ensure balancing between fast transient response and accurate steady-state restoration depending on time protocol. In general, the design guidelines for the parameters of the proposed control system are presented, and the stability analysis based on Lyapunov criteria is presented. The validation of the proposed control is tested by using MATLAB/ Simulink.

Future work will focus on using the second or higher-order low-pass filter to calculate the deviation term, which

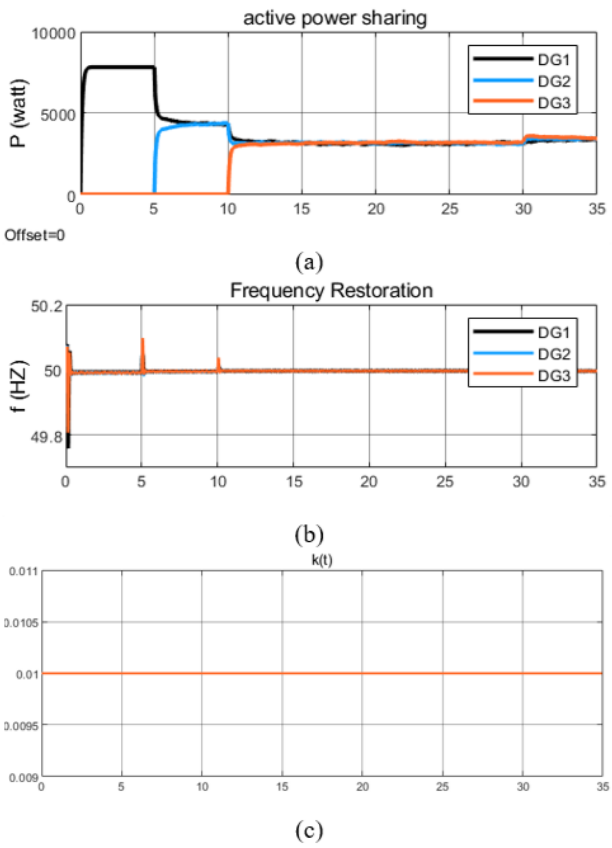

Fig. 13. (a) Active power-sharing of the proposed control scheme for k=0.01, and (b) frequency restoration of the proposed control scheme for k=0.01, (c) time-dependent protocol of parameter k.

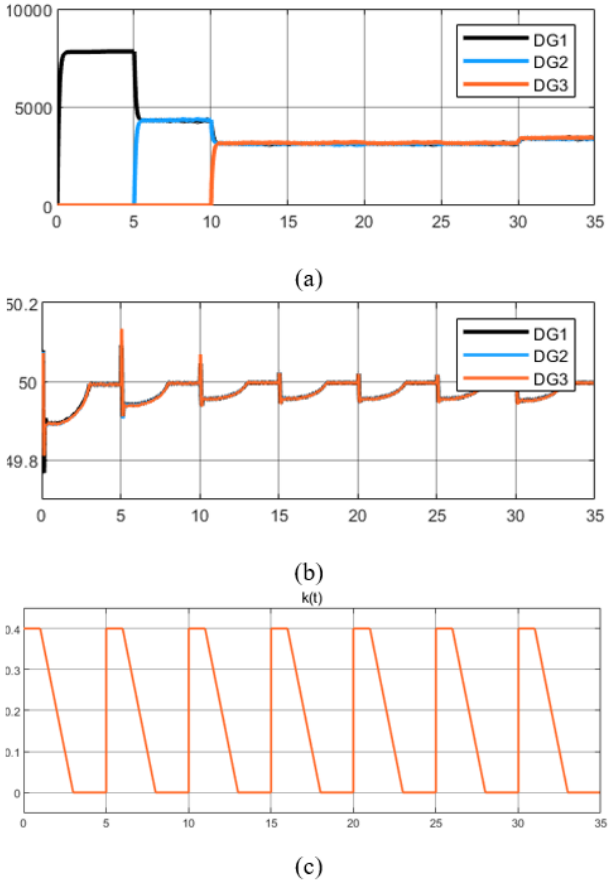

Fig. 14. (a) Active power-sharing of the proposed control scheme is based on a time-dependent protocol, (b) frequency restoration of the proposed control scheme with a time-dependent protocol, and (c) time-dependent protocol of parameter k.

would improve the transient characteristics of the proposed first-order low-pass filter.

Conflict of Interest

The authors have no conflict of relevant interest to this article.

References

[1] M. Chandorkar, D. Divan, and R. Adapa, "Control of parallel connected inverters in stand-alone ac supply systems," *Conference Record of the 1991 IEEE Industry Applications Society Annual Meeting*, pp. 1003–1009 vol.1, 1991.

[2] A. Jasim, B. Hani, A. Flah, V. Bolshev, and L. MIHET-POPA, "A new optimized demand management system for smart grid-based residential buildings adopting renewable and storage energies," *Energy Reports*, vol. 9, pp. 4018–4035, 12 2023.

[3] A. M. Jasim, B. H. Jasim, H. Kraiem, and A. Flah, "A multi-objective demand/generation scheduling model-based microgrid energy management system," *Sustainability*, vol. 14, no. 16, 2022.

[4] B. Naji Alhasnawi, B. Hani, B. Sedhom, and J. Guerrero, "A new communication platform for smart ems using a mixed-integer-linear-programming," *Energy Systems*, pp. 1–18, 07 2023.

[5] S. Hou, J. Chen, and G. Chen, "Distributed control strategy for voltage and frequency restoration and accurate reactive power-sharing for islanded microgrid," *SSRN Electronic Journal*, 01 2022.

[6] I. Poonahela, S. Bayhan, H. Abu-Rub, M. Begovic, and M. Shadmand, "On droop-based voltage and frequency

restoration techniques for islanded microgrids," pp. 1–8, 10 2021.

[7] K. Feng and L. Chunhua, "Distributed hierarchical control for fast frequency restoration in vsg-controlled islanded microgrids," *IEEE Open Journal of the Industrial Electronics Society*, vol. PP, pp. 1–11, 01 2022.

[8] I. Poonahela, A. Krama, S. Bayhan, U. Fesli, M. Shadmand, H. Abu-Rub, and M. Begovic, "Hierarchical model predictive droop control for voltage and frequency restoration in ac microgrids," *IEEE Open Journal of the Industrial Electronics Society*, vol. PP, pp. 1–13, 01 2023.

[9] R. Jackson, S. Aizam, M. Benbouzid, S. Salimin, E. D. M. Khan, E. Garba, and E. Pathan, "A comprehensive motivation of multilayer control levels for microgrids: Synchronization, voltage and frequency restoration perspective," *Applied Sciences*, vol. 10, p. 8355, 11 2020.

[10] J. A. Lopes, C. Moreira, and A. Madureira, "Defining control strategies for microgrids islanded operation," *Power Systems, IEEE Transactions on*, vol. 21, pp. 916 – 924, 06 2006.

[11] A. Tsikalakis, "Centralized control for optimizing microgrids operation," vol. 23, pp. 1 – 8, 08 2011.

[12] J. Guerrero, J. C. Vasquez, J. Alcala, L. Vicuna, and M. Castilla, "Hierarchical control of droop-controlled ac and dc microgrids—a general approach toward standardization," *Industrial Electronics, IEEE Transactions on*, vol. 58, pp. 158 – 172, 02 2011.

[13] H. Liang, B. J. Choi, W. Zhuang, and X. Shen, "Stability enhancement of decentralized inverter control through wireless communications in microgrids," *Smart Grid, IEEE Transactions on*, vol. 4, pp. 321–331, 03 2013.

[14] Q. Shafiee, J. Guerrero, and J. C. Vasquez, "Distributed secondary control for islanded microgrids-a novel approach," *Power Electronics, IEEE Transactions on*, vol. 29, 01 2013.

[15] C. Stefanovic, T. Dragicevic, P. Popovski, J. C. Vasquez, and J. Guerrero, "Robust networked control scheme for distributed secondary control of islanded microgrids," *Industrial Electronics, IEEE Transactions on*, vol. 61, 10 2014.

[16] L. Meng, X. Zhao, F. Tang, M. Savaghebi, T. Dragicevic, J. C. Vasquez, and J. Guerrero, "Distributed voltage unbalance compensation in islanded microgrids by using dynamic-consensus-algorithm," *IEEE Transactions on Power Electronics*, pp. 1–1, 01 2015.

[17] S. Liu, X. Wang, and P. Liu, "Impact of communication delays on secondary frequency control in an islanded microgrid," *IEEE Transactions on Industrial Electronics*, vol. 99, 11 2014.

[18] C. Ahumada, R. Cardenas, D. Saez, and J. Guerrero, "Secondary control strategies for frequency restoration in islanded microgrids with consideration of communication delays," *IEEE Transactions on Smart Grid*, vol. 7, pp. 1–1, 08 2015.

[19] P. Martí, M. Velasco, E. X. Martín, L. García de Vicuña, J. Miret, and M. Castilla, "Performance evaluation of secondary control policies with respect to digital communications properties in inverter-based islanded microgrids," *IEEE Transactions on Smart Grid*, vol. 9, no. 3, pp. 2192–2202, 2018.

[20] M. Shi, X. Chen, J. Zhou, Y. Chen, J. Wen, and H. He, "Frequency restoration and oscillation damping of distributed vsgs in microgrid with low bandwidth communication," *IEEE Transactions on Smart Grid*, vol. 12, no. 2, pp. 1011–1021, 2021.

[21] A. K. Sahoo, K. Mahmud, M. Crittenden, J. Ravishankar, S. Padmanaban, and F. Blaabjerg, "Communication-less primary and secondary control in inverter-interfaced ac microgrid: An overview," *IEEE Journal of Emerging and Selected Topics in Power Electronics*, vol. 9, no. 5, pp. 5164–5182, 2021.

[22] M. Hua, H. Hu, Y. Xing, and J. Guerrero, "Multilayer control for inverters in parallel operation without intercommunications," *IEEE Transactions on Power Electronics - IEEE TRANS POWER ELECT*, vol. 27, pp. 3651–3663, 08 2012.

[23] Y. Wang, Y. Tan, Z. Chen, X. Wang, and Y. Tian, "A communication-less distributed voltage control strategy for a multi-bus ac islanded microgrid," in *2014 International Power Electronics Conference (IPEC-Hiroshima 2014 - ECCE ASIA)*, pp. 3538–3545, 2014.

[24] A. Sahoo, M. Ciobotaru, and J. Ravishankar, "A novel communication-less frequency restoration technique in droop controlled inverter-based islanded ac microgrid," in *2018 IEEE International Conference on Power Electronics, Drives and Energy Systems (PEDES)*, pp. 1–6, 2018.

[25] H. Xin, L. Zhang, Z. Wang, D. Gan, and K. P. Wong, "Control of island ac microgrids using a fully distributed

approach," *IEEE Transactions on Smart Grid*, vol. 6, no. 2, pp. 943–945, 2015.

[26] H. Xin, R. Zhao, L. Zhang, Z. Wang, K. P. Wong, and W. Wei, "A decentralized hierarchical control structure and self-optimizing control strategy for f-p type dgs in islanded microgrids," *IEEE Transactions on Smart Grid*, vol. 7, no. 1, pp. 3–5, 2016.

[27] M. Kosari and S. H. Hosseinian, "Decentralized reactive power sharing and frequency restoration in islanded microgrid," *IEEE Transactions on Power Systems*, vol. 32, no. 4, pp. 2901–2912, 2017.

[28] A. Jasim and B. Jasim, "Grid-forming and grid-following based microgrid inverters control," *Iraqi Journal for Electrical and Electronic Engineering*, vol. 18, pp. 111–131, 06 2022.

[29] G. Chen, F. L. Lewis, E. N. Feng, and Y. Song, "Distributed optimal active power control of multiple generation systems," *IEEE Transactions on Industrial Electronics*, vol. 62, no. 11, pp. 7079–7090, 2015.

[30] A. Jasim, B. Hani, V. Bureš, and P. Mikulecky, "A new decentralized robust secondary control for smart islanded microgrids," *Sensors*, vol. 22, p. 8709, 11 2022.

[31] N. Lakshminarasamma, S. Augustine, and M. Mishra, "Control of photovoltaic-based low-voltage dc microgrid system for power sharing with modified droop algorithm," *IET Power Electronics*, vol. 9, 03 2016.

[32] J. Yu, C. Dou, and X. Li, "Mas-based energy management strategies for a hybrid energy generation system," *IEEE Transactions on Industrial Electronics*, vol. 63, no. 6, pp. 3756–3764, 2016.

[33] B. Naji Alhasnawi, B. Hani, B. Sedhom, and J. Guerrero, "Consensus algorithm-based coalition game theory for demand management scheme in smart microgrid," *Sustainable Cities and Society*, vol. 74, p. 103248, 08 2021.

[34] B. N. Alhasnawi, B. H. Jasim, W. Issa, and M. D. Esteban, "A novel cooperative controller for inverters of smart hybrid ac/dc microgrids," *Applied Sciences*, vol. 10, no. 17, 2020.

[35] B. Naji Alhasnawi and B. Hani, "A new internet of things enabled trust distributed demand side management system," *Sustainable Energy Technologies and Assessments*, vol. 46, p. 101272, 08 2021.

[36] M. Castilla, J. Miret, J. Matas, L. Garcia de Vicuna, and J. M. Guerrero, "Control design guidelines for single-phase grid-connected photovoltaic inverters with damped resonant harmonic compensators," *IEEE Transactions on Industrial Electronics*, vol. 56, no. 11, pp. 4492–4501, 2009.

[37] B. Ning, Q.-L. Han, and L. Ding, "Distributed secondary control of ac microgrids with external disturbances and directed communication topologies: A full-order sliding-mode approach," *IEEE/CAA Journal of Automatica Sinica*, vol. 8, no. 3, pp. 554–564, 2021.

[38] H. Shi, F. Zhuo, H. Yi, F. Wang, D. Zhang, and Z. Geng, "A novel real-time voltage and frequency compensation strategy for photovoltaic-based microgrid," *IEEE Transactions on Industrial Electronics*, vol. 62, no. 6, pp. 3545–3556, 2015.

[39] B. A. Moser and T. Natschläger, "On stability of distance measures for event sequences induced by level-crossing sampling," *IEEE Transactions on Signal Processing*, vol. 62, no. 8, pp. 1987–1999, 2014.